Eurasian Journal of Physics and Functional Materials

Volume 7 | Number 2

Article 2

Pages: 91 - 106

6-22-2023

Research on ferroelectric-piezoelectric properties and relaxor phase transition characteristics of PSLZT-BMT ceramics

N.V. Thinh
College of Sciences, Hue UniversityUniversity of Technology and Education, The University of Danang ,Viet Nam

L.D. Vuong
School of Engineering and Technology – Hue University ,Viet Nam

D.V. On
College of Sciences, Hue University ,Viet Nam

T.V. Chuong
College of Sciences, Hue University ,Viet Nam

L.V. Truong Son
University of Science and Education, The University of Danang ,Viet Nam

See next page for additional authors

Recommended Citation

Thinh, N.V.; Vuong, L.D.; On, D.V.; Chuong, T.V.; Son, L.V. Truong; Dat, T.N.; Son, L.V. Thanh; and Tung, V.T. (2023) "Research on ferroelectric-piezoelectric properties and relaxor phase transition characteristics of PSLZT-BMT ceramics," *Eurasian Journal of Physics and Functional Materials*: Vol. 7: No. 2, Article 2.
DOI: https://doi.org/10.32523/ejpfm.2023070202

Research on ferroelectric-piezoelectric properties and relaxor phase transition characteristics of PSLZT-BMT ceramics

Authors

N.V. Thinh, L.D. Vuong, D.V. On, T.V. Chuong, L.V. Truong Son, T.N. Dat, L.V. Thanh Son, and V.T. Tung

Eurasian Journal of Physics and Functional Materials

2023, 7(2), 91-106

Research on ferroelectric-piezoelectric properties and relaxor phase transition characteristics of PSLZT-BMT ceramics

N.V. Thinh[1,2], L.D. Vuong[*,3],
D.V. On[1], T.V. Chuong[1], L.V. Truong Son[4],
T.N. Dat[4], L.V. Thanh Son[4], V.T. Tung[1]

[1]College of Sciences, Hue University, Hue City, Viet Nam

[2]University of Technology and Education, The University of Danang, Da Nang City, Vietnam

[3]School of Engineering and Technology – Hue University, Hue City, Viet Nam

[4]University of Science and Education, The University of Danang, Da Nang City, Vietnam

e-mail: ldvuong@hueuni.edu.vn

DOI: **10.32523/ejpfm.2023070202**
Received: 11.04.2023 - after revision

(1-x)[(Pb $_{0.94}$ Sr $_{0.05}$ La $_{0.01}$)(Zr $_{0.54}$ Ti $_{0.46}$) $_{0.9975}$ O $_3$]-x[Bi(Mn $_{1/2}$ Ti $_{1/2}$)O $_3$] ceramics with x in the range of 0–0.05 mol were successfully synthesized following the conventional solid-phase route. The materials were thoroughly investigated to study their structural phase, microstructure, ferro-piezoelectric characteristics, and dielectric behavior. The addition of BMT to PSLZT contributed to the transition of the tetragonal phase to the rhombohedral phase and an increase in the mechanical quality coefficient Q_m of the material. The value of the electromechanical coupling coefficient k_p =0.66, the value of k_t =0.53, the value of the piezoelectric constant d_{33} =643 pC/N was obtained in the undoped PSLZT ceramics. The component 0.97PSZT–0.03BMT exhibited properties similar to those of hard piezoelectric ceramics. The electromechanical coupling factor k_p was calculated to be 0.59, the value of k_t was calculated to be 0.48, the piezoelectric constant d_{33} was calculated to be 446 pC/N, the mechanical quality factor Q_m was found to be 774 and the phase transition temperature T_m was calculated to be 265 ° C. The ceramic component shows promise for use in practical power ultrasonic applications.

Keywords: the mechanical quality factor; PSZT-BMT; piezoelectricity; electrical properties; ultrasonic applications

Introduction

The $Pb(Zr_{1-x}Ti_x)O_3$-based ceramics (PZT) are now essential functional materials for actuators, ultrasonic motors, and transducers [1, 2]. PZT has attracted immense attention as they are characterized by a high electromechanical coupling factor (k_p), mechanical quality factor (Q_m), piezoelectric constant (d_{33}), Curie temperature (T_c), and low loss values. This helps meet the demands of miniaturization and high power in practice. PZT ceramics often contain two types of doping: acceptor (hard) doping with lower-valence ions like Fe^{3+}, Mg^{2+}, Al^{3+}, Sc^{3+}, etc., and donor (soft) doping with higher-valence ions like La^{3+}, Ta^{5+}, Nb^{5+}, etc. Donor doping has the potential to enhance the lead vacancies while decreasing the concentration of oxygen vacancies, which causes the ceramics to show high strain and strain hysteresis but low mechanical quality. While the ceramics show low strain, and strain hysteresis is still a good mechanical quality factor, acceptor doping can enhance oxygen vacancies. Some PZT ceramics have donor and acceptor ions co-doped into them to improve their electrical characteristics. In contrast, straining of the PZT lattice due to the substitution of a smaller Sr atom at the Pb site was thought to be the cause of analogous doping such as Sr^{2+}, leading to an increased dielectric permittivity and a high electromechanical coupling factor [3]. Research on the dielectric and piezoelectric properties focuses on co-doping PSLZT with Sr and La by replacing the A site of the ABO_3 perovskite structure [4-6].

Until now, numerous attempts have been made to enhance the electromechanical characteristics of PZT-based materials [3]. It is challenging to achieve high Q_m, k_p, and d_{33} simultaneously. The most popular approach to meet the aforementioned criterion is to introduce acceptor dopants into soft base materials [7]. This is followed for the case of PZT, where Fe^{3+} ions are substituted for the Zr^{4+}/Ti^{4+} sites by producing acceptor-oxygen vacancy defect dipoles ($Fe^{/} - V$). The addition of perovskites with B-site multivalence ions, such as $Pb(Mn_{1/3}Nb_{2/3})O_3$ (PMN) or $Pb(Mn_{1/3}Sb_{2/3})O_3$ (PMS), is another common technique [7, 8]. This method pins the domain walls using oxygen vacancies created by coexisting Mn^{2+} / Mn^{3+} ions during high-temperature sintering [7, 8]. Unfortunately, the sintering temperature required for the aforementioned composition systems is typically higher than 1250° C. For the use of multilayer piezoelectric devices, it is very challenging to find ceramics based on them that have excellent piezoelectric and electromechanical properties and lower sintering temperatures [7, 8]. Furthermore, the use of Nb_2O_5 and Sb_2O_3 would definitely increase the cost of manufacture.

Bi-based perovskite compounds have high T_c and good ferroelectric properties [2, 9, 10]. Additionally, the decrease in sintering temperature would benefit from the addition of Bi-based perovskites to PZT [2]. $Bi(Mn_{1/2}Ti_{1/2})O_3$ is expected to function similarly to PMN and PMS, as previously described. The effect of the addition on the electrical properties and densification of PZT ceramics has never been reported in the literature. In this study, a new ternary solid solution ceramic of PZT was developed following the conventional mixed-oxide method. Particular attention was paid to the variation of the ternary system's dielectric,

ferroelectric, and electromechanical characteristics.

Method

Material preparation

The piezoelectric ceramic system is represented by the formula

$$\text{(1-x)}[(Pb_{0.94}Sr_{0.05}La_{0.01})(Zr_{0.54}Ti_{0.46})_{0.9975}O_3] - x[Bi(Mn_{1/2}Ti_{1/2})O_3].$$

It is abbreviated as PLSZT-xBMT with x in the range 0.00–0.05 mol. The system was prepared following the solid phase reaction method. The initial components are oxides obtained from Daejung, Korea: PbO (99%), ZrO_2 (99%), TiO_2 (98%), $SrCO_3$ (98%), La_2O_3 (99%), Bi_2O_3 (99%), MnO_2 (98%). After being weighed according to the described procedure, the mixture of components was milled for 20 h with zirconia balls in an ethanol medium. Afterward, the powder was calcined for 2 h at 850° C at a heating rate of 300° C/h. Over the course of 20 h, zirconia balls and ethanol were used to re-mill the calcined powder. A uniaxial press was used, a load of 150 MPa was applied, and the discs were pressed in a hardened stainless steel die (diameter: 12 mm; thickness: 1.5 mm). The green ceramic discs were then sintered at 1150° C for 2 h at a heating rate of 300° C/h. Following this, the samples were cooled to room temperature at a rate of 300° C/h.

Characterization

The crystalline structure of sintered ceramics was analyzed using the X-ray diffraction (XRD) technique (D8-Advanced, BRUKER AXS) at room temperature. The surface morphology was studied using (SEM, JEOL-5300) the scanning electron microscopy technique. The grain size and size distribution of the samples were determined via SEM image analysis performed using ImageJ. The densities of the samples were measured following the Archimedes method using ethanol. The silver pastes were swept on both sides of the sample and heated at 500° C for 30 min to develop an electrode for electrical measurements. Dielectric properties were obtained by measuring the temperature dependencies of the capacitance and phase angle (HIOKI 3532) of the samples in the temperature range of $30–350^\circ$ C. To check piezoelectric responses, the specimen was poled in a 120° C silicone oil bath by applying a DC electric field of 3.5 kV/mm for 30 min. Following this, the samples were cooled to room temperature. The specimens were aged for 24 h before testing. The electromechanical factors (k_{ij}) and the mechanical quality factor Q_m were determined following a resonance method (Agilent 4396B and RLC HIOKI 3532). The values were calculated using a formula in the IEEE standard. The piezoelectric constant (d_{33}) was determined using a d_{33} meter (YE2730A, Sinocera). Ferroelectric properties were determined following the Sawyer-Tower circuit method.

Results and discussion

We examined the results obtained using the thermal gravimetric (TG) and thermal analysis (DTA) techniques. The PSLZT-BMT powder was analyzed to determine the calcination temperature (Figure 1 (a)). The TG curve shows a linear decline in the overall mass of the powder under study. However, the DTA curve presents an endothermic peak between 776.42 and 848.09° C, which is associated with ion evaporation.

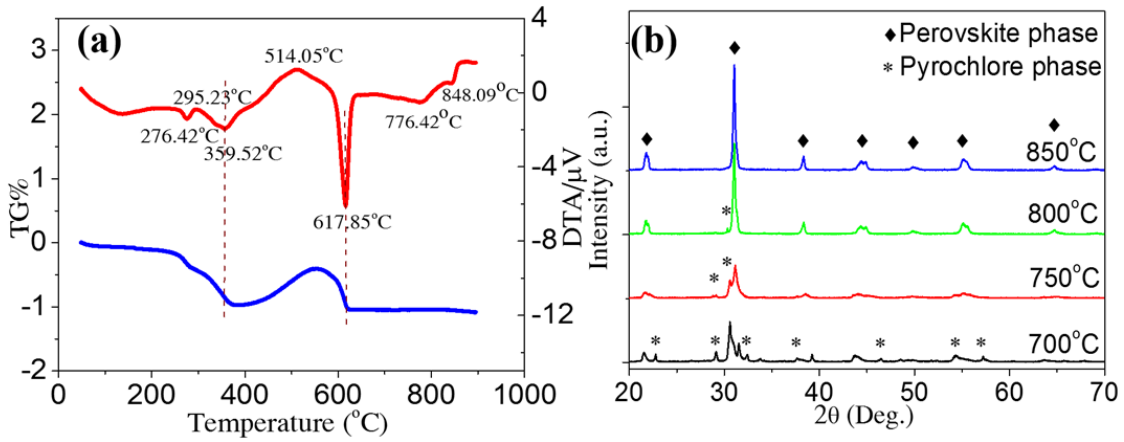

Figure 1. (a) TG/DTA curve and (b) X-ray diffraction pattern of PSLZT-BMT materials.

The mixture of materials after grinding is calcined at different temperatures from 700 to 850° C to accurately determine the phase formation temperature of PSLZT-BMT materials. Figure 1 (b) depicts the material's structural phase in relation to the calcination temperature. The findings demonstrate that the material does not fully form at temperatures below 850° C; the pyrochlore phase is present in the sample under these conditions. The material entirely transitioned into a peroskite structure when the temperature increased to 850° C. As a result, 850° C is selected as the preheating temperature for the PSLZT-BMT material, similar to the study of [9].

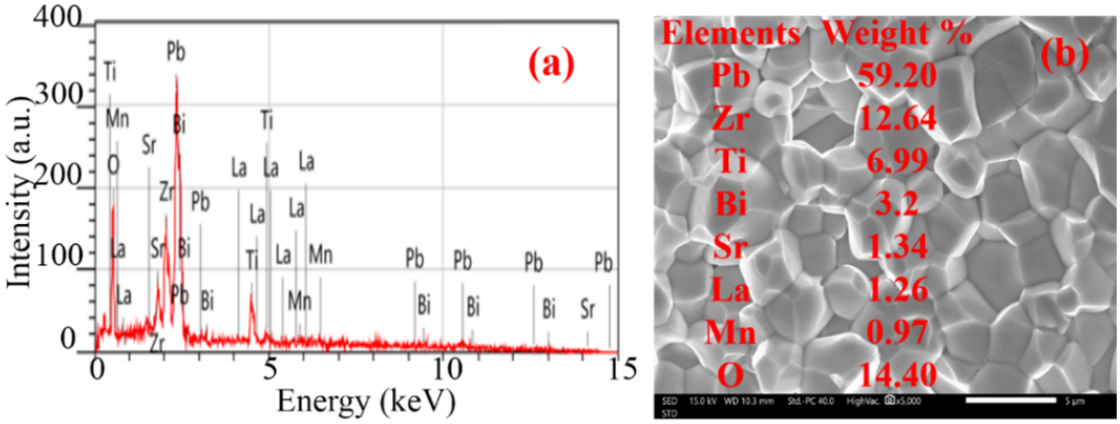

Figure 2. EDS analysis results for PSLZT-BMT material ceramic.

The chemical composition of the sintered PSLZT-BMT ceramic was determined by the EDS technique, and the respective mass percents of Pb, Zr, Ti, Bi, Sr, La,

Mn, and O are presented in Figure 2. It should be noted that the chemical composition of ceramic obtained by EDS technique reflects the general formula with errors within the allowable range, similar to the study of [1].

Table 1.
Density, relative density, densification, and total shrinkage of PSLZT-BMT ceramics as a function of the BMT content.

Sample (mol)	Density (g/cm^3)	Relative density (%)	Densification factor
0.00	7.75	98.48	0.95
0.01	7.70	97.80	0.92
0.02	7.65	97.11	0.90
0.03	7.63	96.88	0.89
0.04	7.60	96.48	0.88
0.05	7.58	96.28	0.87

The densification factor (DF) of the PSLZT-BMT ceramics sintered at 1150° C is calculated using equation (1) as follows:

$$DF = \frac{\rho_m - \rho_g}{\rho_t - \rho_g}, \tag{1}$$

where ρ_t is the theoretical density, ρ_m is the measured density, and ρ_g is the density of the unsintered green pellets [11, 12]. Shrinkage measurements were conducted to check the diameters of both pre-sintered samples using equation (2) as follows:

$$D_{shrinkage} = \left(\frac{d_0 - d_s}{d_0}\right) \times 100\%, \tag{2}$$

where (d_o) and (d_s) are the diameters of the green and sintered pellets, respectively [11]. The density coefficient reaches the maximum value at the PSLZT composition without BMT, and it then decreases with an increase in the BMT content. The positive density coefficient represents the shrinkage of the ceramic system at the sintering temperature of 1150° C [12, 13]. Table 1 shows the rate of shrinkage of the ceramic system as a function of the BMT content. The trend of density change of ceramic at different temperatures is similar to that of the density factor. As the BMT content increased, the density of the samples decreased from 7.75 to 7.58 g/cm^3, and the relative density decreased in the range of 98.48%–96.28%.

The crystal structures of the PSLZT-BMT samples are shown in Figure 3 (a) as a function of the BMT concentrations in the 2θ range of $20–60^\circ$. All samples exhibited typical perovskite structure without any impure phases, indicating that Bi^{3+} and $(Mn_{1/2}Ti_{1/2})^{3+}$ fully diffused into the lattice and formed solutions. Solid solutions were formed with PSLZT [14]. Analysis of the XRD patterns recorded in the ranges of $20.5–22.5^\circ$ (Figure 3 (b)) and $43–46^\circ$ (Figure 3 (c)) revealed that in the BMT content range of 0–0.05 mol, the ceramics were characterized by a mixed rhombohedral (R3 m)–tetragonal (P4 mm) phase with $(001)_T$, $(100)_R$, $(100)_T$, and $(002)_T$, $(200)_R$, and $(200)_T$ reflections, respectively. The

results show that with an increase in the BMT content, the intensity of the $(001)_T$, $(002)_T$ peaks decreases and the intensity of the $(100)_R$, $(200)_R$ peaks increased. This indicated a phase shift (from tetragonal to rhombohedral) with an increase in the BMT content in the range of 0–0.05 mol. The change in the crystal structure could be related to the substitution of the Bi^{3+} ions for the A site ions in the perovskite structure. The radius of Bi^{3+} is smaller than that of Pb^{2+}. Thus, the substitution of the Bi^{3+} ions for Pb^{2+} ions entering into the main crystal phase causes shrinkage of the crystal cell and distortion of the crystal lattice [15].

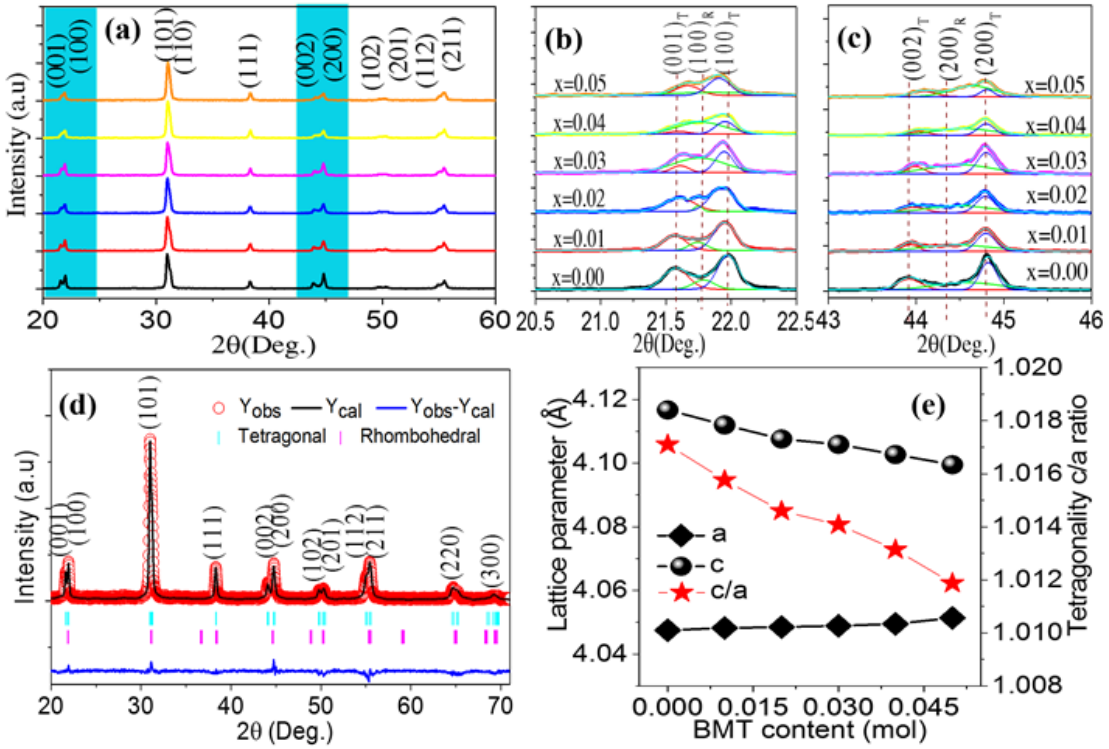

Figure 3. XRD patterns of PSLZT-BMT ceramics at various contents of BMT (a) 2θ =20 °÷ 60 °, (b) 2θ =20.5 °÷ 22.5 °, (c) 2θ = 43 °÷ 46 °, (d) Rietveld-refined XRD patterns of x=0.03, and (e) The lattice constants a, c, and the tetragonal ratio c/a as a function of the BMT content.

In addition, Figure 3 (d) shows the presence of the tetragonal crystal symmetry (P4 mm) in the samples. It was confirmed by the Rietveld purification technique performed using the FullProf software. The lattice constants corresponding to the PSLZT-BMT materials obtained are shown in Figure 3 (e). The results show that the lattice constant (a) increases slightly in the range of 4.0475–4.0514 as the concentration of BMT increases from 0.00 to 0.05. The lattice constant (c) decreases under the same conditions. The ratio of the tetragonal phase (c/a) of the material decreases with an increase in the BMT content, which proves that the content of the tetragonal phase decreases under these conditions. The tetragonal and rhombohedral phase content of the PSLZT-BMT materials at different BMT values is shown in Figure 4. The intensities of the overlapping triplet peaks range from $(200)_T$, $(200)_R$ and $I(002)_T$ in the range 2θ =43 ÷ 46° is used through expression (1) as follows:

$$\%R = \frac{I_{(200)R}}{I_{(200)T} + I_{(200)R} + I_{(002)T}}, \tag{3}$$

$$\%T = 100 - \%R, \tag{4}$$

The results presented in Figure 4 show that the component without BMT is primarily the tetragonal phase and the rhombohedral phase content is approximately 17.96%. Similar results were reported by Volkan Kalem et al. [16], who co-doped Sr and La and the $PbZr_{0.54}Ti_{0.46}O_3$ ceramics. The increased content of BMT doped into PSLZT induces an increase in the rhombohedral fraction. When the content of impurity in BMT reached x=0.05 mol, the symmetry of the perovskite structure gradually changed from tetragonal to rhombohedral. The %T and %R were approximately 54.34% and 45.66%, respectively. From these results, it was concluded that the doping of $(Mn_{1/2}Ti_{1/2})^{3+}$ in the B site of the formulation of these ceramics shifted the morphological phase transition to the Ti-rich region. The incorporation of Mn^{2+} into the B site of the perovskite structure stabilized the rhombohedral phase against the tetrahedral phase [7].

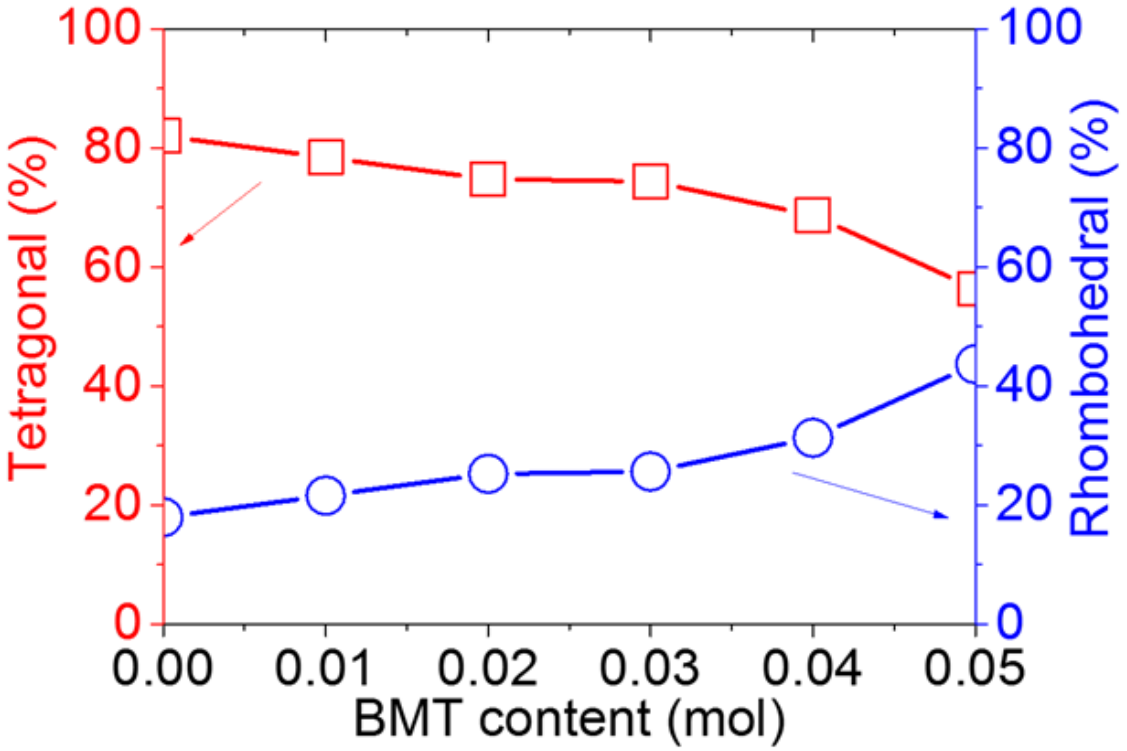

Figure 4. (a) TG/DTA curve and (b) X-ray diffraction pattern recorded for PLSZT-materials.

The microstructure and surface morphology of the PSLZT-BMT material components with x=0–0.05 mol values are presented in Figure 5. Simultaneous doping of Bi^{3+} and Mn^{2+} affected the microstructure and average grain size of PSLZT materials. PLSZT composition devoid of BMT impurities was studied, and it was observed that the ceramic has good crystallinity with clean grain boundaries. The average grain size was approximately 3.04 µm (Figure 5 (a)). As the impurity content increased, the microstructure of the particles changed, and the average particle size decreased from approximately 3.04 µm to 1.76 µm when x changed from 0.0 mol to 0.05 mol (Figure 5 (a)–(f)). The inhibition of grain growth is attributed to the difficult diffusion process that accompanies

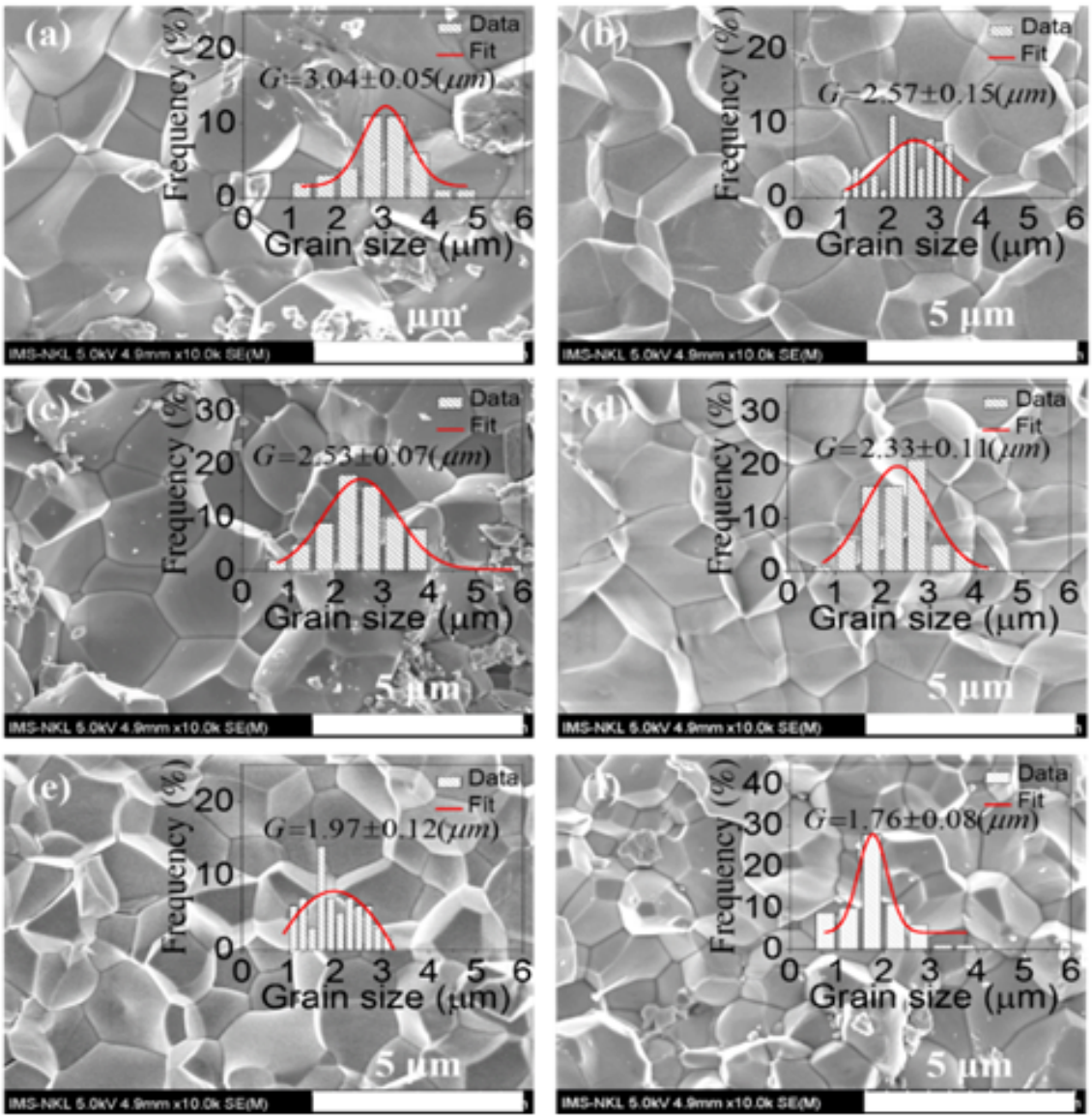

Figure 5. Surface morphologies of the PSLZT-BMT ceramics observed using the SEM technique at various contents of BMT (a) x=0.00 mol, (b) x=0.01 mol, (c) x=0.02 mol, (d) x=0.03 mol, (e) x=0.04 mol, and (f) x=0.05 mol.

the process of Mn-induced lattice contraction [4]. The microstructure accurately reflects the density of the samples (Table 1). The relative density reached the maximum value of approximately 98.48% at the non-BMT component.

To determine the piezoelectric properties of PSLZT-BMT ceramics, the resonance vibration spectra of the components were measured at room temperature by varying the BMT content (Figure 6). The resonance spectra were analyzed, and the values of resonant frequency f_R, anti-resonance frequency f_A, and minimum impedance values Z_{min} were determined (Table 2). Figure 6 presents the frequency-dependent impedance plot generated based on the amplitude and phase angle of PSLZT-BMT ceramic. The resonant and anti-resonant frequencies of the materials tend to shift toward the high-frequency regions as the BMT impurity increases. This clearly reflects the increase in the extent of ceramic shrinkage as a function of the BMT concentration. In addition, the phase angle varies with the frequency of the evaluated material. The results reveal that the phase angle

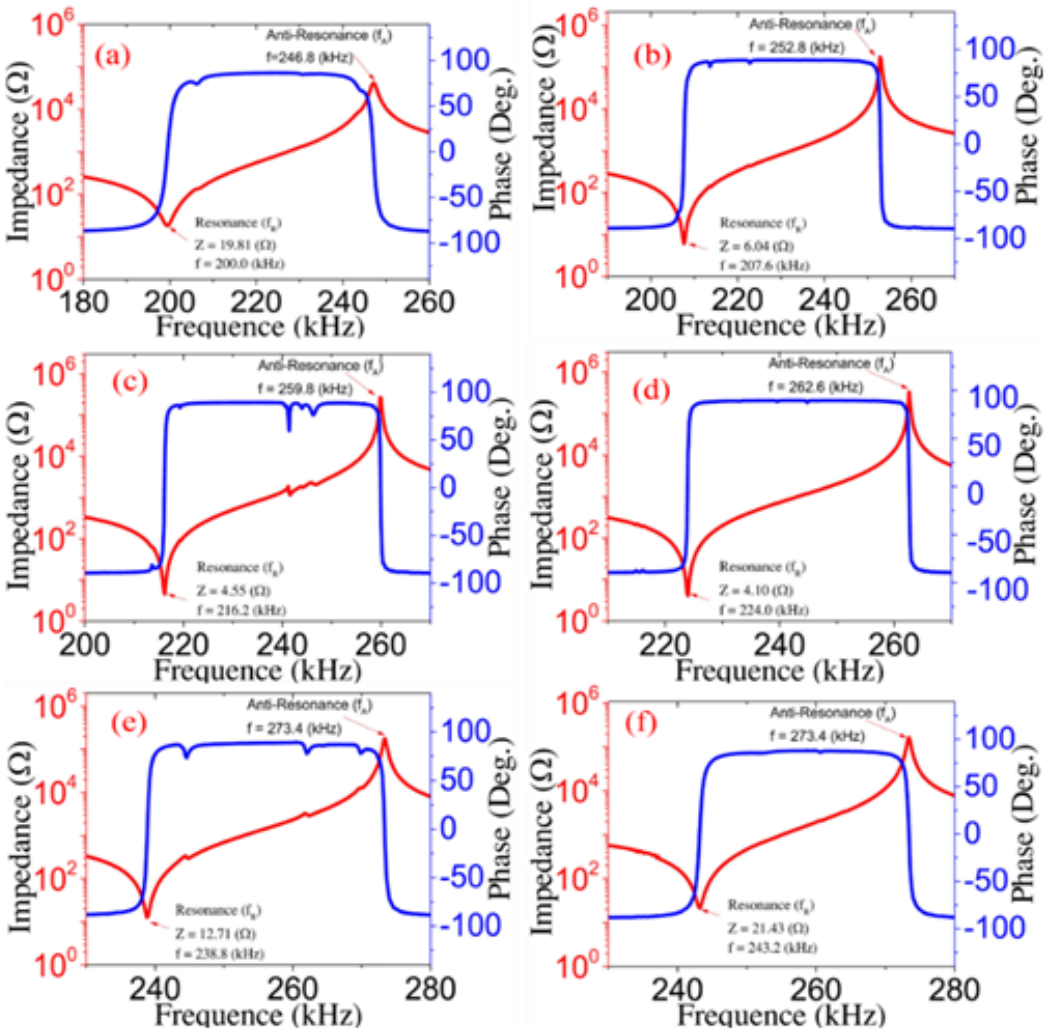

Figure 6. The radial resonance spectral profiles recorded for the PSLZT-BMT ceramics with various contents of BMT (a) x=0.00 mol, (b) x=0.01 mol, (c) x=0.02 mol, (d) x=0.03 mol, (e) x=0.04 mol, and (f) x=0.05 mol.

of ceramics in the mid-resonant-anti-resonance frequency range remains close to $+90^{\circ}$. According to the impedance resonance graph, the obtained PSLZT-BMT ceramic shows good piezoelectric properties [3]. The piezoelectric parameters of the sample, such as electromechanical coupling coefficient k_{ij}, piezoelectric coefficients d_{ij}, and mechanical quality coefficient Q_m, were determined according to the piezoelectric standard IRE61-87.

Table 2.
Physical parameters of PSLZT-BMT ceramics.

x (mol)	f_r (kHz)	f_a (kHz)	Z_{min}	k_p	k_{31}	k_t	d_{31} (pC/N)	d_{33} (pC/N)	Q_m
0.00	200.0	246.8	19.81	0.66	0.33	0.53	179	643	90
0.01	207.6	252.8	6.04	0.65	0.32	0.50	158	554	354
0.02	216.2	259.8	4.55	0.63	0.31	0.49	130	499	628
0.03	224.0	262.6	4.10	0.59	0.29	0.48	120	446	774
0.04	238.8	273.4	12.71	0.55	0.27	0.47	87	369	413
0.05	243.2	273.4	21.43	0.52	0.25	0.45	78	336	294

The influence of Mn^{2+} and Bi^{3+} doping on the dielectric and piezoelectric properties of the ceramics based on PSLZT was investigated. The changes in these properties as a function of the BMT content are presented in Table 2. Apparently, the addition caused interesting changes in the electromechanical properties. This can be attributed to conflicting individual effects caused by Mn^{2+} and Bi^{3+}. The changes occurring in the electromechanical properties of PSLZT ceramics doped with different BMT contents are shown graphically in Figure 7 (b)–(c). The electromechanical coupling coefficient k_{ij} and piezoelectric constant d_{ij} change in the same way and tend to decrease as the content of BMT impurity increases. The electromechanical coupling coefficients k_p, k_t, and k_{31} and the piezoelectric coefficients d33 and d31 reach the maximum values at the non-BMT component. The values are recorded to be 0.66, 0.53, 0.33, 643 pC/N, and 179 pC/N, respectively. The addition of BMT to PSLZT causes a transition from the tetrahedral to the rhombohedral region with a dominant tetragonal phase and a gradual transition to a region with a high rhombohedral phase. This causes the piezoelectric degradation of the material when the corresponding BMT concentration is in the range of 0.01–0.05 mol.

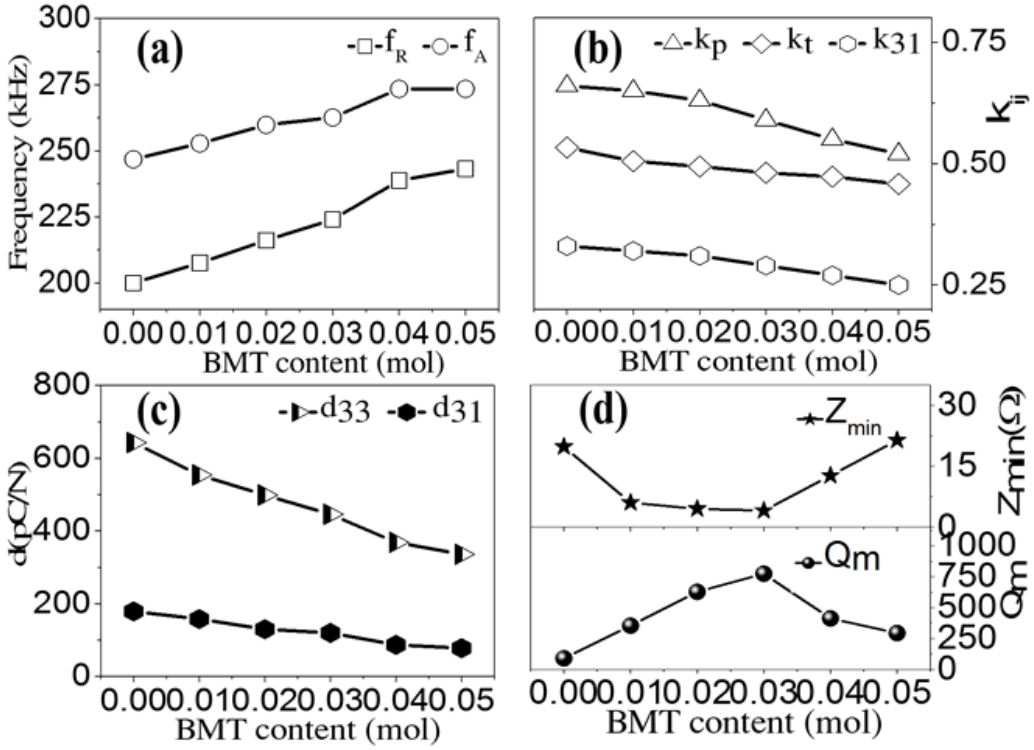

Figure 7. Piezoelectric characteristics of the PSLZT-BMT-based ceramics.

The mechanical quality factor Q_m and the Z_{min} value obtained from the resonant tool spectrum of the material under different BMT values are shown in Figure 7(d). The trend in the changes in the Z_{min} and Q_m values are opposite when the BMT content increases. The relationship between Z_{min} and the mechanical quality factor Q_m can be expressed using expression (2) as follows:

$$Q_m = \frac{f_A^2}{2\pi f_r (f_A^2 - f_R^2) Z_{min} C'}, \tag{5}$$

where f_R is the resonance frequency, f_A is the anti-resonance frequency, Z_{min} is the impedance at the resonance frequency, and C is the capacitance. According to the analytical results presented in Figure 7 (d), the impedance of the components with contents in the range of 0.01–0.03 mol decreased and became lower than the values corresponding to the non-BMT component. The minimum value of 4.1 Ω was reached at x=0.03 mol. Following this, the impedance increased with an increase in the concentration of the impurities. The mechanical quality coefficient of the PSLZT-BMT ceramic system is calculated according to the expression (5) presented in Table 2. The Q_m value of the material increases as a function of x in the range of 0–0.03 mol and reaches a large value of 774 at x=0.03 mol. Following this, the value of Q_m decreases with an increase in the BMT content. According to Volkan Kalem et al. [16], this effect can be potentially attributed to the reduction in the grain size of the ceramic. The motion of the domain wall is also affected by the grain size [4]. Since the grain boundaries act as additional pinning points, the motion of the domain wall is inhibited by an increase in the grain size. The decrease in the mechanical quality factor when the BMT content is greater than 0.03 mol can be related to the rapid decrease in the density of the material [8].

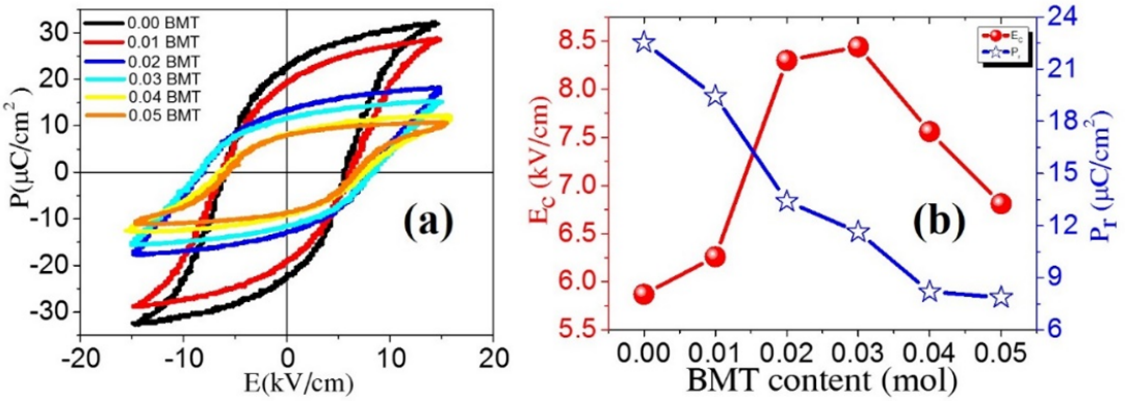

Figure 8. (a) Hysteresis loops of PSLZT-BMT samples and (b) P_r and E_c as a function of BMT content.

Figure 8 (a) presents the polarization loops versus field delay plots for PSLZT-BMT samples containing varying amounts of doped BMT. It can be seen that all hysteresis loops of the sample exist in a saturation state, which is characteristic of typical ferroelectric materials. For the PSLZT component not doped with BMT, the hysteresis loop is characteristic of soft piezoelectric material with a large residual bias and a small resistive electric field. The changing pattern of residual polarization decreases in the range of 22.54–7.87 μC/cm^2 when the BMT concentration is in the range of 0–0.05 mol. At the same time, the resistive electric field value E_c initially increased to 8.44 kV/cm when the concentration was 0.03 mol. Following this, the value decreased as the doping content increased (Figure 8 (b)).

The change in the shape of the ferroelectric hysteresis ring corresponding to the PSLZT-BMT system with an increase in the doping content follows the characteristic of hard piezoelectric ceramics. This is related to the defect dipoles generated by the acceptor ions and the oxygen vacancy generated by the substitution of Bi^{3+} ions for the A site of Pb^{2+} and $(Mn, Ti)^{3+}$ to the B site of

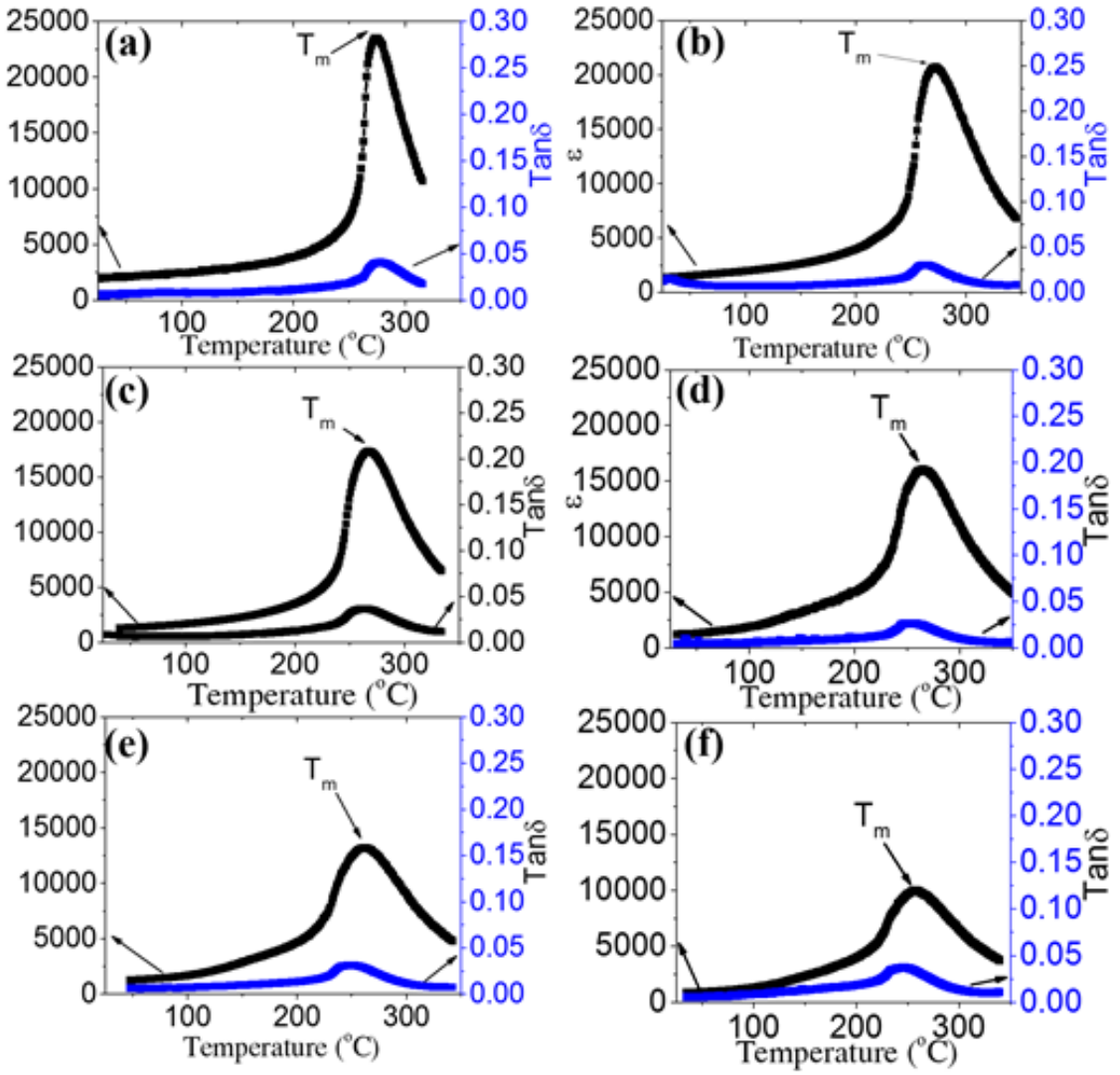

Figure 9. Temperature-dependent dielectric constant ϵ and dielectric loss $\tan\sigma$ recorded measured at 1 kHz for the PSLZT-BMT ceramics.

$(Zr, Ti)^{4+}$ ion. Thus, they prevent the orientation of the ferroelectric domains resulting in a reduction in the residual polarization of the material. In addition, oxygen vacancies can also be generated due to the loss of oxygen from the lattice during the process of high-temperature sintering. Oxygen vacancies trapped inside the domain-oriented pinning domain walls cause electrical surges in the resistance field of the material. It also results in an increase in the value of the mechanical quality factor Q_m. As shown in Figure 8(b), the Q_m value of the material decreases with an increase in the BMT content (≤ 0.05 mol). The particle size reduction effect caused the pinning of the domain wall motion and the decrease in the polarization values.

The temperature dependence of the dielectric constant (ϵ) and dielectric loss ($\tan\delta$) of the PSLZT-BMT ceramic samples at 1 kHz is presented in Figure 9. At 1 kHz, the dielectric constant ϵ_{max} of PSLZT reached the maximum value of 23579. Following this, the value decreased in the range of 20706–9991 when the doping content increased in the range of 0.01–0.05 mol (Figure 9 (a–f)). The decreasing trend of the dielectric constant ϵ is thought to be associated with the

decrease in the mean grain size, degree of uniformity, and density of the ceramic samples. The high density, large grain size, and improved crystallinity of the ceramic samples result in high ϵ. In addition, the width of the peaks ϵ(T) can be explained by a diffuse phase transition, one of the key features of relaxed ferroelectrics. According to Ullah et al. [17], the high density, large grain size, and improved crystallinity of the ceramic samples result in high dielectric constants.

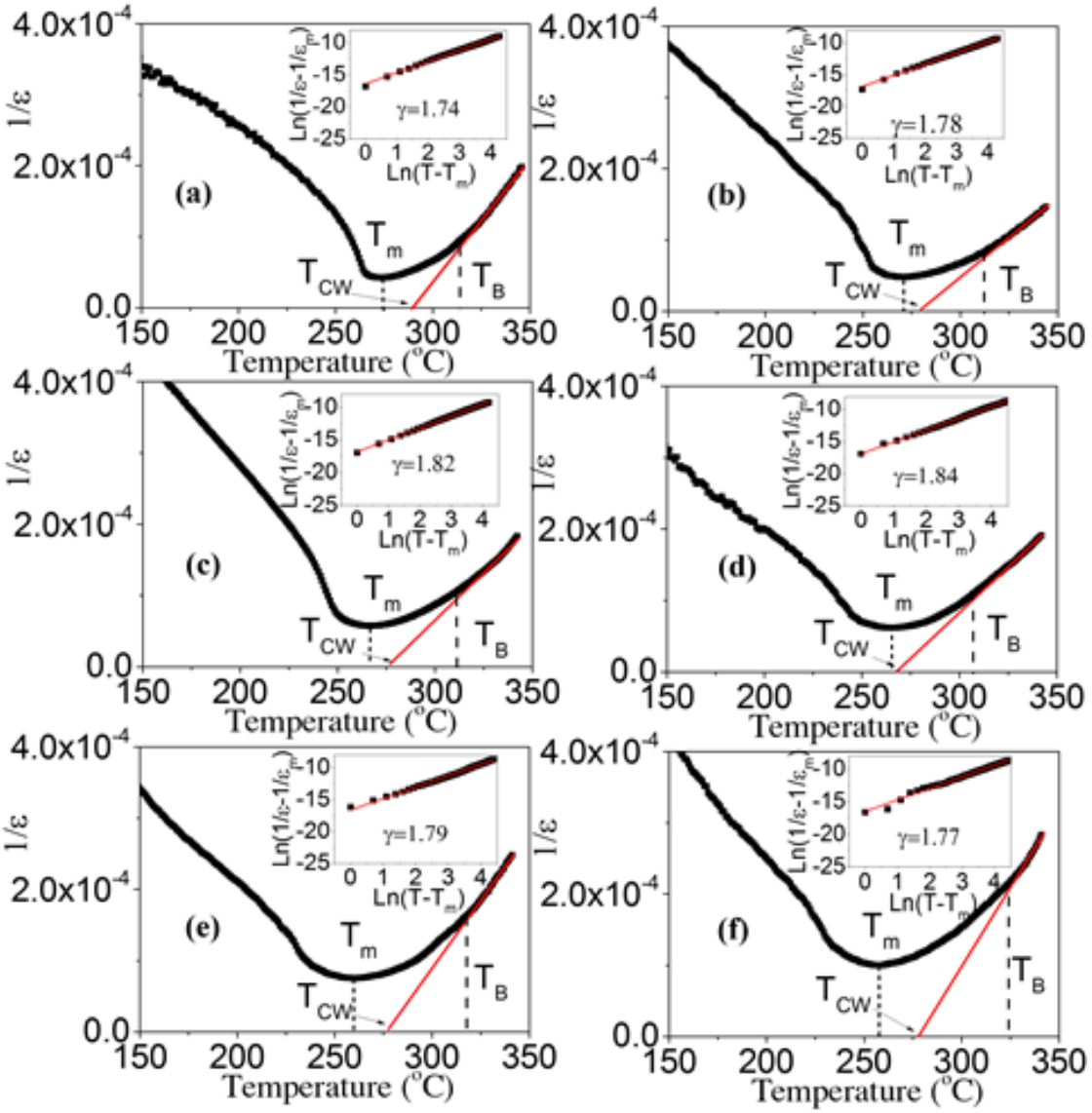

Figure 10. Curie-Weiss dependence of the dielectric constant of the PSLZT-BMT materials.

Figure 10 presents the temperature dependence of the inverse dielectric constant associated with the PSLZT-BMT material. The corresponding matches were obtained using the modified Curie Weiss law as follows:

$$\frac{1}{\epsilon} - \frac{1}{\epsilon_{max}} = \frac{(T - T_m)^{\gamma}}{C} (1 \leq \gamma \leq 2), \tag{6}$$

where ϵ_{max} is the maximum value of the dielectric constant at the phase transition temperature T_m, γ is the degree of diffuseness, and C is the Curie constant. The right-hand corner of Figure 10(a–f) shows the diffusivity values (γ) evaluated

by plotting $\ln(1/\epsilon - 1/\epsilon_{max})$ versus $\ln(T - T_m)$ at 1 kHz. The γ values of the PSLZT-BMT material are 1.74, 1.78, 1.82, 1.84, 1.79, and 1.77 when the doping content x varies as 0.0, 0.01, 0.02, 0.03, 0.04, and 0.05 mol, respectively (Table 3). It can be seen that the value of γ increases as the BMT content increases to 0.03 mol. Thus, the process of phase transition becomes more diffuse with an increase in the BMT content, and this can be attributed to larger disturbances in the samples. The observations can be attributed to the diffuse paraelectric-ferroelectric phase transition occurring under conditions of increased γ values. However, the γ value decreased as the BMT content increased. This can be potentially attributed to the fact that the solubility limit of Bi^{3+} and Mn^{2+} ions in PSLZT-BMT-based ceramic is approximately 0.03 mol. As the BMT value increases, a fraction of ions located at the grain boundary inhibits grain growth, resulting in structural heterogeneity and a decrease in the γ values. Analysis Figure 10 yields the values of T_m, T_B, T_{C-W}, and Curie constant (C) (Table 3). It can be seen that the values of T_B, T_{C-W}, and C depend on BMT concentration. The trend of dependence is the same as the trend observed for g values. The value of the C is calculated to be in the range of 1.35×10^7–2.17×10^7. The phase transition temperature ^{TM} tends to decrease from 274 to 257 as the doping concentration increases in the range of 0–0.05 mol. This can be attributed to the particle size reduction effect of the material.

Table 3.
Dielectric parameters calculated for the PSLZT-BMT samples.

Sample (mol)	T_m (°C)	T_B (°C)	T_{C-W} (°C)	ϵ_r (at RT)	ϵ_{max} (at T_m)	γ	C ($\times 10^7$)
0.00	274	318	290	1731	23579	1.74	1.35
0.01	271	315	280	1490	20706	1.78	2.10
0.02	267	311	275	1146	17352	1.82	2.13
0.03	265	306	268	1158	16145	1.84	2.17
0.04	261	318	277	769	13218	1.79	1.58
0.05	257	324	278	716	9991	1.77	1.49

The temperature and frequency dependence of the dielectric constant of the PSLZT-BMT samples is shown in Figure 11 (a). The results show that when the frequency increases in the range of 1–1000 kHz, ϵ_{max} tends to decrease, and the value moves to a higher temperature region. The dielectric loss increases and shifts toward T_m (Figure 9). It can be seen that this effect is a typical feature of relaxor materials [2, 10]. This can be potentially attributed to the fact that when the measurements are made at 1 kHz, the total dielectric constant is the sum of the different polarization mechanisms, including directional polarization, spatial charge polarization, electronic polarization, and recovery polarization. However, when the measurement frequency is high, the contributions of directional polarization, spatial charge polarization, and relaxation polarization decrease. Under these conditions, the electronic polarization primarily contributes to the total dielectric constant, resulting in a decrease in the ϵ value.

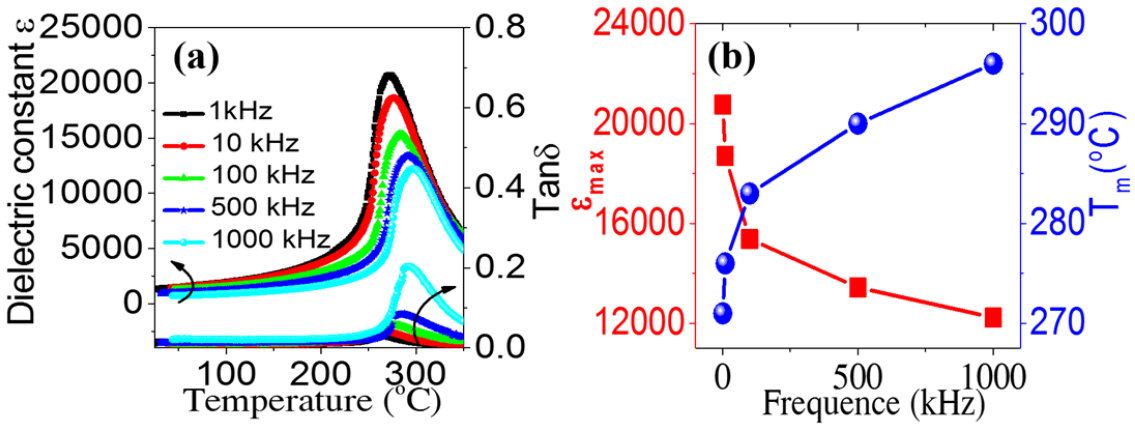

Figure 11. Temperature and frequency-dependence of dielectric constant and dielectric loss of the PSLZT-BMT materials at 1, 10, 100, and 1000 kHz.

Conclusion

A group of piezoelectric ceramic components

$$(1\text{-}x)[(Pb_{0.94}Sr_{0.05}La_{0.01})(Zr_{0.54}Ti_{0.46})_{0.9975}O_3] - x[Bi(Mn_{1/2}Ti_{1/2})O_3]$$

with x in the range of 0–0.05 mol was successfully synthesized by conducting conventional solid phase reactions. The content of BMT contributes to the changes in the phase structure of the material. The mixed tetrahedral phase transformed into the rhombohedral phase, and the dominant tetrahedral phase transformed into the dominant rhombohedral phase. The grain size of the material decreased in the range of 3.04–1.76 μm, and the relaxor phase transition dielectric properties were generated with an increase in the BMT content in the range of 0.00–0.05 mol. As a result, soft and hard piezoelectric ceramics with excellent properties were obtained. Soft ceramic PSLZT systems devoid of BMT are characterized by good electromechanical parameters. The value of the electromechanical coupling coefficient k_p was 0.66, the value of k_t was 0.53, the value of the piezoelectric constant d_{33} was 643 pC/N, the value of the mechanical quality factor Q_m was 90, and the phase transition temperature T_m was 274° C. The 0.97PSLZT–0.03BMT ceramics exhibited the properties of hard piezoelectric ceramics with k_p =0.59, k_t =0.48, d_{33} =446 pC/N, Q_m =774, and T_m = 265° C. This hard ceramic can potentially be used in the field of ultrasonic power.

References

[1] D.A. Quang, L.D. Vuong, Journal of Science: Advanced Materials and Devices **7**(2) (2022) 100436. [*CrossRef*]
[2] L.D. Vuong, Journal of Materials Science: Materials in Electronics **33** (2022) 6710-6721.[*CrossRef*]
[3] H.-T. Kim et al., Journal of Asian Ceramic Societies **9**(3) (2021) 1083-1090. [*CrossRef*]
[4] V. Kalem, M. Timucin, Journal of the European Ceramic Society **33**(1) (2013) 105-111. [*CrossRef*]

[5] L.D. Vuong et al., Journal of Electronic Materials **47**(10) (2018) 5944-5951. [*CrossRef*]
[6] L.D. Vuong, P.D. Gio, Journal of Modern Physics **5**(14) (2014) 1258-1263. [*CrossRef*]
[7] K.P. Rema, V. Kumar, Journal of the American Ceramic Society **91**(1) (2008) 164-168. [*CrossRef*]
[8] S.-W. Kim, H.-C. Lee, Materials **15**(20) (2022) 7070. [*CrossRef*]
[9] N. Truong-Tho, D. Le Vuong, Journal of Materials Science: Materials in Electronics **32**(12) (2021) 16601-16611. [*CrossRef*]
[10] L.D. Vuong et al., Journal of Materials Science: Materials in Electronics **31** (2020) 18056-18069. [*CrossRef*]
[11] M. Alkathy et al., Journal of Alloys and Compounds **762** (2018) 49-61. [*CrossRef*]
[12] N.T. Tho, L.D. Vuong, Journal of Electroceramics **45** (2020) 47-55. [*CrossRef*]
[13] H. Naceur et al., Journal of Advanced Ceramics **3** (2014) 17-30. [*CrossRef*]
[14] Zh. Yu et al., Ceramics International **43** (2017) 14996-15001. [*CrossRef*]
[15] J.G. Chen et al., Materials Research Innovations **14** (2010) 234-237. [*CrossRef*]
[16] V. Kalem et al., Ceramics International **37** (2011) 1265-1275. [*CrossRef*]
[17] A. Ullah et al., Current Applied Physics **10** (2010) 1367-1371. [*CrossRef*]